Journal of Electroanalytical Chemistry 780 (2016) 360–366

Contents lists available at ScienceDirect

Journal of Electroanalytical Chemistry

journal homepage: www.elsevier.com/locate/jelechem

Optical and structural study of electrodeposited zinc selenide thin films

Murilo F. Gromboni *, Lucia H. Mascaro

Department of Chemistry, Federal University of São Carlos, Washington Luiz, km 235, 13565-905, São Carlos, SP, Brazil

ARTICLE INFO

Article history:
Received 15 July 2015
Received in revised form 13 March 2016
Accepted 19 April 2016
Available online 30 April 2016

Keywords:
Zn-Se
Electrodeposition
Thin films
Semiconductors
Photocurrent

ABSTRACT

This paper reports a study of the electrodeposition of ZnSe on Pt electrodes in a sulfuric acid solution at pH 2.0 with the purpose of producing stoichiometric films. The film's properties were evaluated for different Zn/Se ratios. The films were deposited at different potentials (−0.2, −0.5, −0.7 and −0.9 V) and characterized by X-ray Diffraction (XRD), Scanning Electron Microscope (SEM), X-ray Fluorescence (XRF) and non-contact 3D optical profilometry (3D-OP). Band gap, photocurrent, carrier number and flat-band potentials were determined. The films with higher photocurrent, carrier number, and crystallinity were obtained at −0.9 V; these films were p-type and presented 1:1 stoichiometry.

© 2016 Elsevier B.V. All rights reserved.

1. Introduction

The electrodeposition process is a popular method used in the coating industry of metals and alloys [1,2]. This technique is an interesting way to obtain films of metals, semiconductors, or composites with thicknesses ranging from nano to micrometer. In addition, this technique is not expensive and is simple, yet capable of producing films of high quality, large area, and various geometric shapes [3]. Regarding semiconductors, there has been a growing interest in the application of binary or ternary semiconductors in photovoltaic devices, especially thin films of chalcogenides [4–6]. These films are usually produced by physical techniques such as vacuum evaporation [7], chemical vapor deposition [8], or sputtering [9]. Despite the advantages of the electrodeposition method, it is not widely used for the production of semiconducting thin films. However, some results have shown that this could be a viable and less expensive alternative to the production of films. For instance, Bhattacharya has obtained a rich Cu-CIGSe film by electrodeposition, which was used in a photovoltaic device and has achieved an efficiency of 14.1% [10].

Binary semiconductors formed with chalcogens such as CdSe, CdTe, ZnSe, and ZnS present interesting features for being cheap and showing a high degree of absorption in photovoltaic and photoelectrochemical cells [11]. In this particular case, these semiconductors have gaps that cover the visible spectrum and have a high degree of optical conversion [12]. Among many binary semiconductors, ZnSe has been identified as an important alternative material to the CdS in electro-junction solar cells. This semiconductor has a band gap of 2.7 eV, and it is capable of emitting light in the blue-green [5]. It is found as a p- [13] or n-type [14] semiconductor. However, while n-type doping of ZnSe is readily achieved, it has been much harder to identify an effective p-type semiconductor. There are several deposition methods for ZnSe thin films, such as the chemical bath deposition [15], photochemical deposition [16], underpotential deposition (UPD) [17], pulsed electrodeposition [18], epitaxial electrochemical deposition (ECALE) [5] and potentiostatic electrodeposition [12]. The problem with the electrodeposition of this material is that the stoichiometric compound (1:1) is rarely obtained, there is always an excess of selenium in the material.

Potentiostatic electrodeposition of ZnSe can be carried out in acid [5,12], alkaline [19,20] or non-aqueous solution [21]. The acid solution is more studied by different authors using ITO [22], Cu [23], Ti [23] and porous Si [24] substrates. Many authors observed that ZnSe crystalline films with Se excess are obtained and that stoichiometry for the Zn:Se ratio can be achieved after annealing treatment [5,25]. The influence of deposition parameters such as deposition potential, Se(IV) and Zn(II) concentration, and temperature of bath on the crystallinity and on the chemical composition of the film has been discussed [5,26,27]. According to Kowalik et al. [5], the electrodeposition of ZnSe can only take place in a narrow potential range. It is limited either by H_2Se formation and hydrogen evolution or insufficient polarization of the electrode to deposit zinc on selenium [27]. On the other side, some authors proposed that Se^{2-} (H_2Se) can react directly with Zn(II) in the solution, forming more ZnSe [12]. An increase in Se(IV) concentration and in the temperature accelerates the process of deposition and thicker films are obtained [27,28]. In most works, the best conditions for ZnSe thin films deposition are a potential between −0.85 and −0.95 V and the temperature between 60 and 70 °C [26]

Despite countless studies on the electrodeposition of ZnSe thin films described in the literature, each presents a type of study. The techniques most commonly used in these works are cyclic voltammetry, SEM,

* Corresponding author.
E-mail address: mgromboni@yahoo.com.br (M.F. Gromboni).

http://dx.doi.org/10.1016/j.jelechem.2016.04.037
1572-6657/© 2016 Elsevier B.V. All rights reserved.

optical measurements, XRD and Mott–Schottky. There is no work with a complete characterization of this system, which should correlate the film properties with its composition. Also, although these films can be applied in solar cells, there is no work that presents photocurrent measurements and number of acceptors and makes a correlation of these values with composition, morphology and roughness of the film such as this work does. Thus, the objective of this work was to evaluate the process of deposition of ZnSe thin films to obtain a stoichiometric compound and correlate the optical and physical properties with different stoichiometries.

2. Experimental

The reagents of analytical grade were SeO_2, $ZnSO_4 \cdot 7H_2O$, NaOH and H_2SO_4 from Sigma Aldrich, which were used directly without further purification. Aqueous solutions were prepared with deionized water taken from a MILLI-Q purification system. For the electrodeposition of films, the solution was prepared with 100 mM $ZnSO_4$ and 1 mM SeO_2 in H_2SO_4 with pH adjusted to 2.0 using NaOH. The photoelectrochemical experiments were performed in 0.1 M ferrocene ($[Fe(C_5H_5)_2]$) + 0.5 M sodium perchlorate ($NaClO_4$) in acetonitrile (CH_3CN). For the electrochemical impedance analysis, a solution of 0.5 M H_2SO_4 with pH adjusted to pH 2.0 was used.

All experiments were performed using and electrochemical cell with three electrodes. The electrodes used were a platinum wire counter electrode and a saturated calomel (SCE) reference electrode which was produced and certified using a Princeton Applied Research model 219995. The potential values were corrected regarding the standard hydrogen electrode (SHE) in all figures (ΔE vs.SHE = +0.25 V; T = 20 °C). The working electrodes were polycrystalline Pt plates with a geometrical area of 1.65 cm^2. Voltammetric experiments started with a cathodic scan at +1.3 V (vs. SCE). The films were prepared using a potentiostatic mode where the electrodeposition potential was chosen from cyclic voltammetric results. The electrode was polarized at different potentials, −0.2, −0.5, −0.7 and −0.9 V (vs. SHE), during 63 min.

Voltammetric scanning, photocurrent, and impedance measurements were performed using a potentiostat SP-150 from Bio-Logic Science Instruments with EC-Lab® V10.12. The photocurrent system was from Newport 66902 with 100 mW cm^{-2} and the cell had a quartz window and 1 cm of optical distance. The temperature during all experiments was maintained at 20 °C using a Polystat® thermostatic bath from Cole-Parmer.

The measurements of the film/electrolyte capacitance were made by superimposing an a.c. potential, oscillating between −0.2 and +0.2 V at a frequency of 5 kHz, on the applied potential (E_{ap}). This oscillating voltage range was chosen to avoid inducing any faradaic currents.

The photocurrent was analyzed using the chronoamperometric technique setting the light on and off and applying 0.2 V more positive than the open circuit potential for 300 s with the chopper period adjusted to 50 s. The films were analyzed by Scanning Electron Micrographs (SEM) and Energy-dispersive X-rays spectroscopy (EDX). SEM images were obtained using a microscope mod 35 VP Zeiss-Supra. Reflectance UV–vis spectra were obtained using a UV–VIS HITACHI U-3900H spectrometer. The band gaps of the films were calculated from transmission studies that investigated the optical absorption properties of the ZnSe films. The optical band gap should obey the following Tauc equation from the plot of $(\alpha h\nu)^2$ vs. photon energy ($h\nu$) [18].

$$(\alpha h\nu)^2 = cte(h\nu - E_g) \quad (1)$$

where α is the absorbance, h is the Planck constant, and ν is the frequency. By plotting $(h\nu)^2$ vs. $h\nu$ we can determine the band gap (E_g).

The X-ray diffraction analysis of the films was obtained with a Bruker D8 Advance diffractometer, using CuK radiation l = 1.5406 Å, voltage of 40 kV and theta-2theta configuration, sweeping angle of 20–65° with a rate of 0006 ° s^{-1}. The surface roughness was evaluated by non-contact 3D optical profilometry (3D-OP) using a multifocal microscope S/M-NEOX, Sensofar-Tech SL, along with the SensoSCAN DCM3D v.3.1 software. Roughness profiles were obtained by filtering the roughness effects for which the wavelength was superior to the selected cut-off length (λc). A cut-off value of 0.800 mm was selected, using a Gaussian type filter, as recommended by the norm ISO 11562:1996 [29]. For the XRF measurements, we used a FISCHERSCOPE® X-RAY XDV® SDD fluorimeter operating with a voltage of 30 kV and 40 W power and with apertures of 3 mm for the electron beam. Data were collected with the software WinFTM 3.2.

3. Results and discussion

3.1. Voltammetric study

A voltammetric study of the deposition and dissolution for individual species (Zn(II) and Se(IV)) and for the mixture (Zn(II) + Se(IV)) was previously performed in order to establish information about the possible range of deposition potentials of ZnSe films. The cyclic voltammograms obtained for 100 mM of Zn(II), 1 mM Se(IV) and for the mixture in pH 2.0 and 200 mV s^{-1} are shown in Fig. 1.

In Fig. 1A the cyclic voltammograms obtained at different cathodic reversing potentials are presented. Basically, three cathodic (C_1, C_2

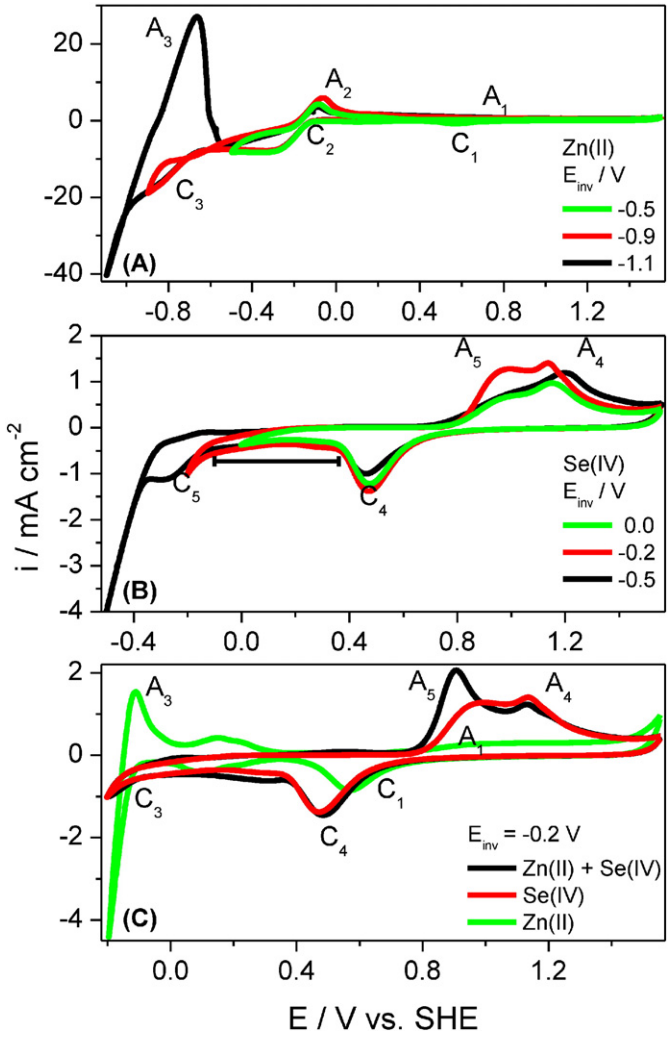

Fig. 1. Cyclic voltammograms for a solution of (A) 100 mM Zn(II), (B) 1 mM Se(IV) changing the cathodic potential of inversion and (C) 100 mM Zn(II) + 1 mM Se(IV) in comparison to Se(IV) and Zn(II). All CVs using 0.5 M H_2SO_4 pH 2.0, Pt substrate and v = 200 mV s^{-1}.

and C_3) and three anodic processes (A_1, A_2, A_3) can be observed. It was possible to relate cathodic and anodic processes by changing the cathodic potential of inversion. The peaks C_1 and A_1, better visualized in Fig. 1(C), green curve, corresponds to the reduction and formation of platinum oxide on the surface of the electrode, respectively [30]. The peaks C_2 and A_2 are defined when the maximum cathodic potential is −0.5 V (green curve) and they are attributed to the formation and oxidation of H_2, they can also be considered to be the result of hydrogen adsorption/desorption from the bulk of the metal [31]. These processes occur at potentials more negative than that for the adsorption of a hydrogen monolayer and they are also observed for the blank solution. At more negative potentials, from −0.7 V, the third process is observed (peaks C_3 and A_3), for which the anodic current increases the more negative the reverse potential is in the cathodic scan. The CVs for the Se (IV) solution are presented in Fig. 1B, where the peak C_4 is observed in a potential slightly more negative than that for peak C_1 in Fig. 1A. This peak corresponds to reduction of the platinum oxide and to Se underpotential deposition (UPD) [32]. The dissolution of Se UPD occurs simultaneously with the formation of platinum oxide and is assigned as peak A_4. In the potential range between +0.4 and −0.1 V the bulk Se deposition was observed; its dissolution process is associated to peak A_5. When the potential is scanned up to −0.5 V, a peak in −0.2 V (C_5) is observed, which is attributed to the reduction of Se bulk to Se^{2-} with the formation of H_2Se. Due to this, in the anodic scan it is observed that the current of peak A_5 decreases. The CVs for pure ions and for the mixture, Se(IV) and Zn(II), are presented in Fig. 1C, where the maximum cathodic potential is −0.2 V. In this potential it is possible to observe the process of formation of the monolayers. It is possible to observe that the curves for the mixture are very similar to those for Se(IV), except regarding the anodic peak A_3. The current of this peak increases in presence of Zn(II), which could be due to the formation of ZnSe or due to the presence of Zn(II) in solution easing the deposition of Se bulk [33]. Another point to note is that processes related to Zn UPD, hydrogen monolayer and formation of H_2, which are observed for the pure Zn(II) solution (potential range 0.3 to −0.2 V), are not noted in the case of the mixture. This is due to deposition happening on Pt, covering the whole surface and inhibiting these processes.

The anodic process (A_5) is associated with the oxidation of $H_{2(g)}$ due to hydrogen bubbles that are generated at negative potentials on the surface and do not detach from the electrode. The processes A_4 and A_1 are also observed, they are related to hydrogen desorption and zinc monolayer at +0.15 V and Pt oxidation at +0.94 V. In the window showed in Fig. 1(C), it is not possible to observe the peaks of dissolution or deposition of zinc; this is only possible in Fig. 1(A) for potentials more negative than −0.9 V. The deposition of Zn bulk (C_7) starts at −0.9 V and the anodic peak A_7 at −0.82 V is correlated with its dissolution.

In order to correlate the cathodic and anodic processes, cyclic voltammograms were obtained for the mixture of Zn(II) + Se(IV) at different cathodic reversing potentials (Fig. 2).

Fig. 2 shows that when the potential is swept towards values more negative than −0.2 V, the anodic peaks related to Se bulk and Se UPD in Fig. 1A and 1C clearly change and only one anodic peak is observed. The current of this peak increases and the potential shifts to more positive values when the cathodic reversing potential is more negative, this behavior characterizes the formation of a bulk film. The shift to a more positive potential indicates that the species that are being oxidized is not the same as that described previously. This occurs because, at more negative potentials, Se(0) is reduced to selenide (Se^{2-}), which chemically reacts with Zn(II) to form zinc selenide. In this case, zinc is not reduced; consequently, is not possible to observe the peaks of deposition and dissolution of Zn, assigned as C3 and A3 in Fig. 1A. Thus, the selenide is incorporated in the ZnSe film and in the anodic scan this species is oxidized from Se^{2-} to Se^{4+}. This behavior indicates that the ZnSe film is formed in more negative

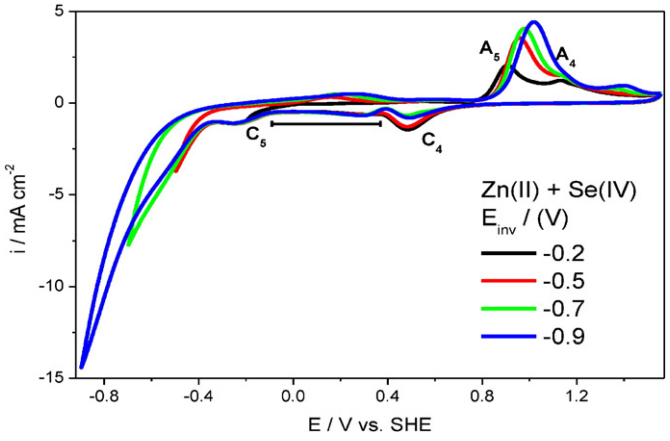

Fig. 2. Cyclic voltammograms for a solution of 100 mM Zn(II) + 1 mM Se(IV) on Pt at different cathodic reversing potentials, v = 200 mV s^{-1}.

potentials, i.e., reduction happens in the region of Se(0) to Se^{2-}. Some authors propose the mechanism below for the formation of ZnSe species [5,14,17,22,27].

$$H_2SeO_3 + 4H^+ + 4e^- \rightarrow Se + 3H_2O \quad (2)$$

$$Zn^{2+} + Se + 2e^- \rightarrow ZnSe \quad (3)$$

$$H_2Se + Zn^{2+} \rightarrow ZnSe \quad (4)$$

Based on voltammetry response, four different potentials were chosen to prepare ZnSe films. Potentiostatic depositions at −0.2, −0.5, −0.7 and −0.9 V were performed during 63 min and the films were characterized by XRD, SEM, XRF, 3D-OP, electrochemical impedance, and UV–vis. All samples had a grayish brown color, which is a characteristic of ZnSe films [22]. It is known that ZnSe films present either gray or red coloration, depending on whether they have an excess of Zn or amorphous Se, respectively [20].

3.2. Physical properties of ZnSe films

The structural properties of electrodeposited ZnSe thin films were investigated by X-ray diffraction using CuK(alpha) radiation with l = 0.154 nm. X-ray diffraction patterns were recorded for ZnSe thin films obtained at different deposition potentials, −0.2, −0.5, −0.7 and −0.9 V, by maintaining the deposition time and bath temperature at 63 min and 20 °C, respectively. Fig. 3 shows the XRD patterns obtained. For reasons of clarity the peak regions marked with numbers 1, 2, 3, 4 and 5 were broadened and shown together with the complete diffractogram.

X-ray diffraction patterns show various diffraction peaks at 39.8°, 39.9° and 46.3°, 46.5°attributed to the Pt (PDF# 87-646) substrate. The Se phase (PDF# 06-0362) was observed in peaks at 42.2°. The Zn phase (PDF# 65-3358) was also observed in peaks at 36.3° and 39.1°. The peaks at 43.2° and 53.4° were attributed to the (220) and (311) planes of cubic ZnSe (PDF# 5-522), respectively. Some authors attribute the peak at 46.3° to the ZnSe (220) [27,34]. When the deposition potential decreases, the films show improved crystalline structure and the intensity of the ZnSe, Zn and Se diffraction peaks increases. The diffraction peaks are somewhat broader, indicating that the crystallite size is small; this is a characteristic of deposits obtained in limiting current conditions. The presence of the peak associated with the Se phase, around 42.2° for all samples, indicates that despite the formation of ZnSe, part of the deposited selenium did not form a ZnSe compound.

For the film obtained at −0.9 V, it was observed that there is an increased intensity and a small displacement of the peaks at 39.8° and 46.3° (insert 2, 4), while peaks at 39.9° and 46.5° disappeared.

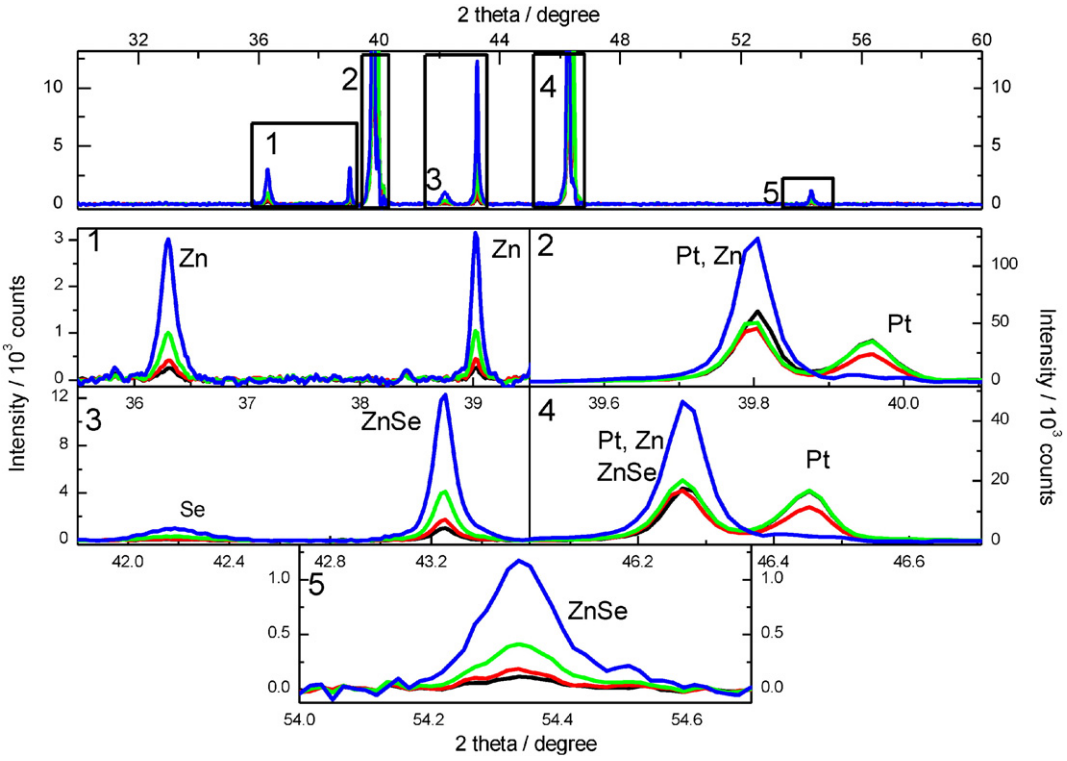

Fig. 3. X-ray diffractograms of ZnSe films electrodeposited at different potentials: −0.45 V (black), −0.75 V (red), −0.95 V (green) and −1.15 V (blue). The insets (1), (2), (3), (4) and (5) show the different peaks that were noted.

This may occur because in this condition there is a significant deposition of zinc, which shows characteristic peaks at approximately 39.8° and 46.3° (Zn PDF # 65-3358). In this condition there is an increased deposition of Zn in the film and it becomes thicker. Also, this may be due to deposition of the ZnSe (220) phase grown this potential when Se^{2-} react directly with the Zn(II) in the solution forming ZnSe [17,22]. Consequently the substrate signal decreases, which could explain why the 39.9° and 46.5° peaks have disappeared.

Fig. 4 shows the scanning electron micrograph at two different magnifications for the films deposited in various conditions. The films are found to exhibit a smooth surface revealing grains covering well the substrate. The deposits mostly present globular agglomerates of ZnSe crystallites. Aggregation of the crystallites forming larger clusters are observed as the deposition potential becomes more negative. The sample obtained in −0.2 V is the one with more homogeneous and compact growth. In −0.9 V, clusters have a cauliflower-type structure and the film is apparently thicker. The SEM results showed that morphology of films is dependent on the deposition potential. Similar results were observed in the literature [5,12,35].

The rugosity of ZnSe films was evaluated from 3D-OP and the composition, molar ratio and thickness of ZnSe films were evaluated from XRF data. The values are presented in Table 1. The results showed that the Zn content in the film increases when deposition potential is more negative. This behavior is in agreement with the results of cyclic voltammetry, which pointed out that the Zn deposition occurred at more negative potentials. This behavior is in agreement with the results of cyclic voltammetry, which pointed out that the Zn deposition occurred at more negative potentials. It can be concluded that at −0.2 and −0.5 V, where there are Se excess, the reaction occurs according to the Eq. (1). These results are according Riveros et al. where Zn/Se stoichiometric ratios of 20/80 was observed for the as-grown for film deposited at −0.7 V [22]. At more negative potential the Zn^{2+} reduction starts and the reaction can occur via Eqs. (2) or (3), so the incorporation of an excess of elemental selenium in the film lowered.

Both the thickness and rugosity of the film also increase for more negative deposition potentials, confirming the SEM results. Considering that stoichiometric films can provide better characteristics, the potential of −0.9 V is more appropriate to obtain films with this composition. The Zn/Se ratio increase is explained considering that, at the more negative potential, more Se^{2-} was formed, which can react with Zn directly forming more ZnSe [17,22].

These results is not according that reported in the literature, where it is recommended that the deposition potential should not be more negative than −0.9 V. Because the crystallinity, stoichiometry and stability of the film is worse in this condition [39]. It is can be due the different experimental condition used for these authors, as deposition temperature, ion concentration and electrolyte.

3.3. Optical characterization

The band gap is a characteristic of semiconductor materials, so its values were obtained from diffuse reflectance spectra for the studied samples. The representation of Wood-Tauc hα vs $(\alpha h\nu)^2$ is given at Fig. 5, where it is possible to observe that the band gap values practically do not change with the deposition potential. The mean value of 2.73 ± 0.01 eV was obtained and it was close to the values found in the literature for ZnSe films deposited by others methods [16,35,36]. These values are higher than what is expected for massive ZnSe, which is in the order of 2.6 eV [37]. The higher band gap value for electrodeposited ZnSe can be due to the formation of nanocrystalline structures, as observed in the XRD analysis [38]. One should also remember that that despite the changes observed in the morphology and composition of ZnSe films obtained in different conditions, the band gap determined for different authors are very similar, with values from 2.5 to 2.7 eV [13,39]. In conclusion, the ZnSe phase is predominant in the sample, because pure Se has a much smaller band gap, near 1.7 eV. Pure Zn phase as a metal should not change the band gap of the ZnSe film. It should be noted that even for samples obtained at −0.2 and −0.5 V,

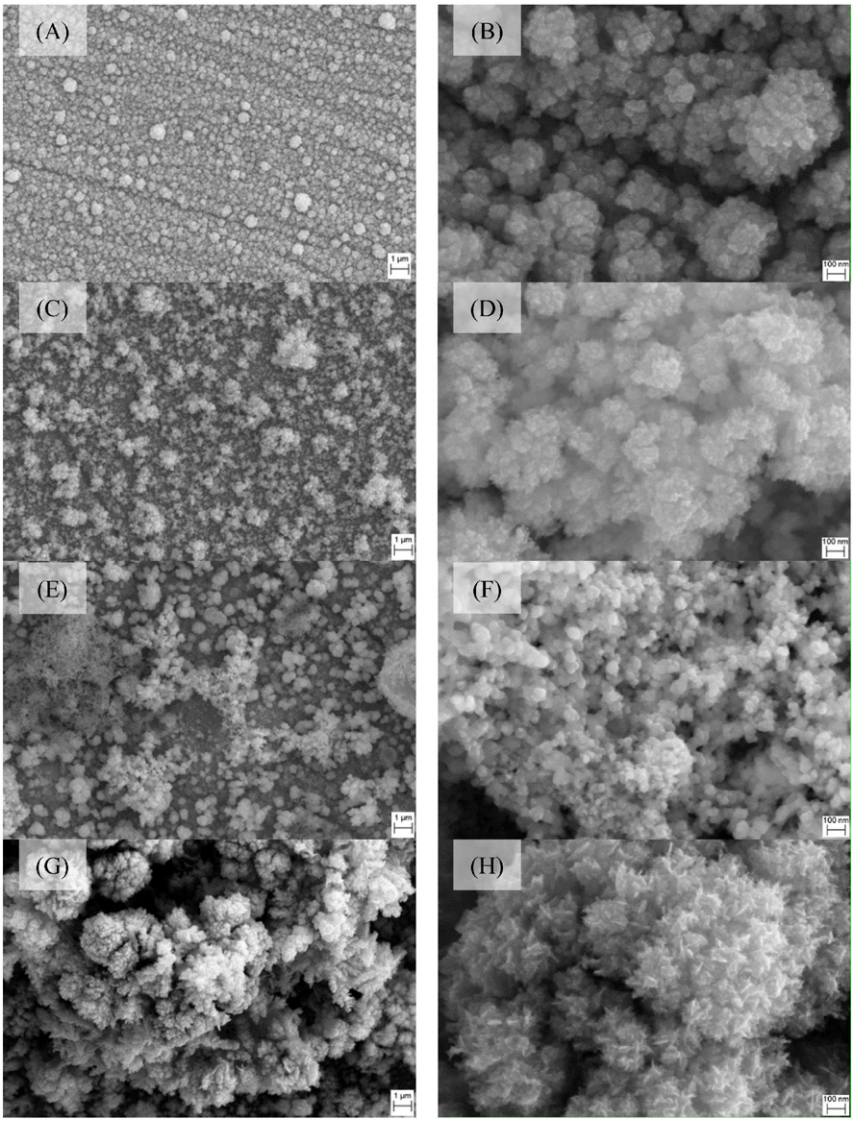

Fig. 4. SEM micrographs of ZnSe films at different magnifications and electrodeposited at different potentials −0.2 V (A, B), −0.5 V (C, D), −0.7 V (E, F) and −0.9 V (G, H).

where there is excess of Se, the band gap obtained is from the ZnSe. This occurs because the absorptivity coefficient of ZnSe is much greater than that of pure Se.

There are few papers that relate the band gap value with ZnSe composition [39,40] and most of these papers do not present in which composition the band gap was measured. Dhanasekaran et al. [39] observed that the band gap energy of films decreased from 2.54 to 2.52 eV when the deposition potential was changed from −0.85 to −0.95 V, respectively. Pingale et al. [40] found that the band gap of ZnSe decreased from 2.69 to 2.52 eV as the Zn/Se ratio decreased from 0.993 to 0.570.

Considering that ZnSe films can be employed in photovoltaic cells, photocurrent of the films deposited at different potentials was also evaluated. The photocurrents were analyzed using the chronoamperometric technique with the light on and off, applying 0.2 V more positive than the open circuit potential for 300 s with the chopper period adjusted to 50 s. The experiments were performed using 0.1 M of ferrocene ($[Fe(C_5H_5)_2]$) in acetonitrile (CH_3CN) and 0.5 M sodium perchlorate ($NaClO_4$). Fig. 6 presents the chronoamperometric response, with the light off and on, and the photocurrent values are given in Table 1. As shown in Table 1, there was a significant variation in photocurrent for the evaluated samples. The values of the photocurrent varied up to six times; however, the roughness of the film ranged to only 1.5×, indicating that the increase in photocurrent is not only due to increased surface area. A correlation between the increase in the photocurrent and the composition of the film can be made. With increasing zinc content in the film, there was an increase in the photocurrent; being the maximum value obtained for the film with a molar ratio of Zn:Se of 1:1. Compared to the band gap data, which was not observed to have changed in value

Table 1
Composition, thickness, rugosity and optical properties of ZnSe films obtained from different deposition potentials.

Sample	$\%_{at}$Zn	$\%_{at}$Se	Zn/Se ratio	Rugosity/nm	Thickness/nm	I_{PC}/μA cm^{-2}	$N_a/10^{15}$ cm^{-3}	E_{FB}/V
−0.2 V	13.0	86.0	0.16	108	242	112	7.0	0.98
−0.5 V	21.9	78.1	0.28	113	460	143	8.5	0.94
−0.7 V	37.3	62.7	0.59	125	521	313	19.0	1.01
−0.9 V	52.0	48.0	1.08	156	1612	674	122.6	1.06

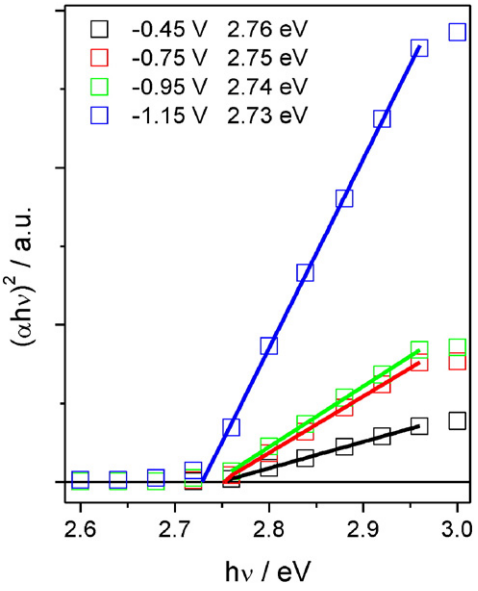

Fig. 5. Plot of hν vs. $(\alpha h\nu)^2$ for ZnSe samples obtained at −0.2 V (black square); −0.5 V (red circle); −0.7 V(green triangle) and −0.9 V (blue triangle) from UV–Vis spectra.

with the composition of the film, it can be said that this property is much more sensitive to the experimental conditions under which the films were obtained.

The electronic properties of the film were evaluated by capacitance measurements of the film at different applied potentials. The flat band potential (E_{fb}), the charge carriers density ($N_{A,D}$) and the semiconductor type (n- or p-) were determined using the Mott–Schottky equation given below [13]:

$$\frac{1}{C^2} = \left(\frac{2}{e_0 \varepsilon \varepsilon_0 N_{AD}}\right)\left(E_{ap} - E_{fb} - \frac{K_b T}{e_0}\right)$$

where C is the observed capacitance, e_0 the elementary charge (1.6022×10^{-19}C), N_{AD} the number of acceptors and/or donors per cm^3 in the semiconductor, ε_0 the permittivity of free space (8.8542×10^{-14} F cm^{-1}), ε the semiconductor dielectric constant (8.7 for ZnSe), E_{ap} the applied potential, E_{fb} the flat band potential, K_b the Boltzmann (1.3804×10^{-23} J K^{-1}) constant, and T the absolute temperature (293 K).

Using a Mott–Schottky graph, the N_A can be calculated from the slope and the E_{fb} can be obtained from the extrapolation to $C_{SC}^{-2} = 0$. The measurements of the film/electrolyte capacitance were made by superimposing an a.c. potential, oscillating between −0.2 and +0.2 V at a frequency of 5 kHz, on the applied potential (E_{ap}). The solution used was 0.5 M H_2SO_4.

The Mott–Schottky graph and N_A and E_{fb} values, for ZnSe films obtained at different potentials, can be seen in Fig. 7 and Table 1.

Because the slope was negative in all cases, it is possible to conclude that all obtained films were p-type semiconductors. Similar results were observed in the literature [13]. The average value of E_{fb} was 1.00 ± 0.05 V, which did not change with deposition potential.

The number of acceptors increased almost twenty times when the deposition potential changed from −0.2 to −0.9 V, probably due to defects in the crystalline material network and excess of Se in the film. It is observed that the materials with more crystallinity, by XRD analysis, and the more stoichiometric were the ones that had higher values of N_A, since it is easier when the electron-hole pair is separated. Comparing the values obtained with other values already reported in the literature, it can be seen that the results observed for films deposited at −0.9 V presented values of N_A similar to those obtained by other authors [13,41].

4. Conclusions

This paper showed that the composition of ZnSe electrodeposits significantly varied with the chosen deposition potential, with the Zn content increasing for more negative potentials. The morphology, photocurrent, and electronic properties were also dependent on electrodeposition conditions. On the other hand, the band gap and flat band potential properties were not sensitive to the film composition.

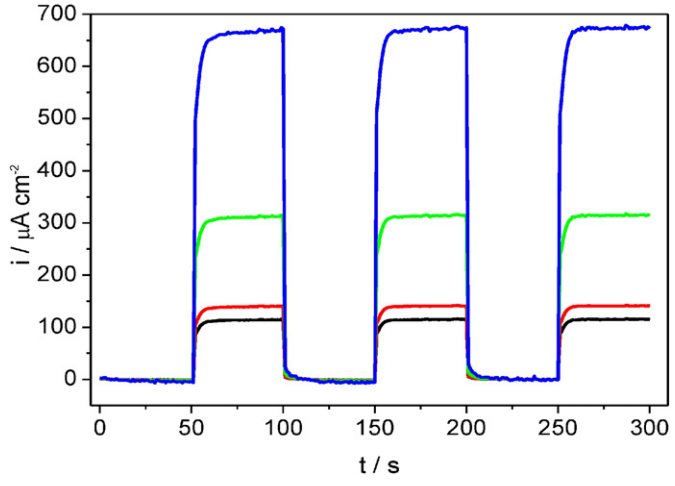

Fig. 6. Chronoamperometry in light and dark applying E = +0.20 V for 300 s in 0.1 M ferrocene +0.5 M $NaClO_4$ in acetonitrile. Equilibrium time 1800 s, $t_{chopper}$ = 50 s. For ZnSe samples deposited in −0.2 V (black), −0.5 V (red), −0.7 V (green) and −0.9 V (blue).

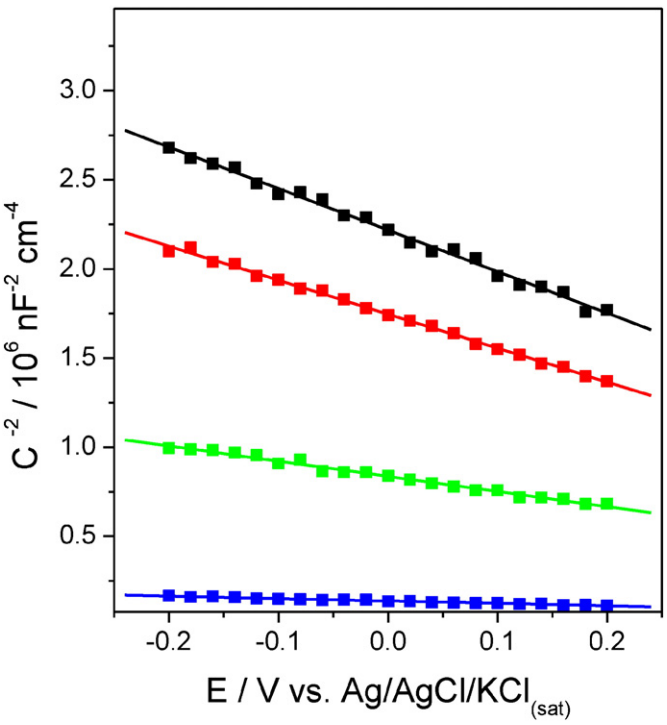

Fig. 7. Mott Schottky plot of ZnSe samples deposited in −0.2 V (black), −0.5 V (red), −0.7 V (green) and −0.9 V (blue).

The higher photocurrent, carrier number, and the more crystalline films were obtained at −0.9 V; these films presented 1:1 stoichiometry. The results indicate that it is possible to obtain stoichiometric p-type ZnSe thin films by electrodeposition at low temperature without post annealing treatment. For the first time a correlation was made between composition, morphology, roughness, photocurrent and number of acceptors of ZnSe coatings. It was demonstrated that the films presented suitable properties for application in photovoltaic devices.

References

[1] U. Erb, Electrodeposited nanocrystals: synthesis, properties and industrial applications, Nanostruct. Mater. 6 (1995) 533–538, http://dx.doi.org/10.1016/0965-9773(95)00114-X.

[2] M. Datta, D. Landolt, Fundamental aspects and applications of electrochemical microfabrication, Electrochim. Acta 45 (2000) 2535–2558, http://dx.doi.org/10.1016/S0013-4686(00)00350-9.

[3] I.M. Dharmadasa, J. Haigh, Strengths and advantages of electrodeposition as a semiconductor growth technique for applications in macroelectronic devices, J. Electrochem. Soc. 153 (2006) G47–G52, http://dx.doi.org/10.1149/1.2128120.

[4] K.R. Murali, M. Balasubramanian, Characteristics of pulse plated $Cd_xZn_{1-x}Se$ films, Curr. Appl. Phys. 10 (2010) 734–739, http://dx.doi.org/10.1016/j.cap.2009.08.018.

[5] R. Kowalik, P. Zabinski, K. Fitzner, Electrodeposition of ZnSe, Electrochim. Acta 53 (2008) 6184–6190, http://dx.doi.org/10.1016/j.electacta.2007.12.009.

[6] R.M. Clark, B.J. Carey, T. Daeneke, P. Atkin, M. Bhaskaran, K. Latham, I.S. Coleb, K. Kalantar-zadeh, Two-step synthesis of luminescent MoS2–ZnS hybrid quantum dots, Nanoscale 7 (2015) 16763–16772, http://dx.doi.org/10.1039/C5NR04790K.

[7] N. Sabli, Z.A. Talib, W.M.M. Yunus, Z. Zainal, H.S. Hilal, M. Fujii, Effect of argon gas on photoelectrochemical characteristics of film electrodes prepared by thermal vacuum evaporation from synthesized copper zinc tin selenide, Int. J. Electrochem. Sci. 8 (2013) 10910–10920 (WOS:000326501300001).

[8] P.J. Wright, B. Cockayne, The organometallic chemical vapour deposition of ZnS and ZnSe at atmospheric pressure, J. Cryst. Growth 59 (1982) 148–154, http://dx.doi.org/10.1016/0022-0248(82)90316-5.

[9] R.A. Wibowo, W.S. Kim, E.S. Lee, B.M., K.H. Kim, Single step preparation of quaternary $Cu_2ZnSnSe_4$ thin films by RF magnetron sputtering from binary chalcogenide targets, J. Phys. Chem. Solid 68 (2007) 1908–1913, http://dx.doi.org/10.1016/j.jpcs.2007.05.022.

[10] R.N. Bhattacharya, 14.1% CuIn1-xGaxSe2-based photovoltaic cells from electrodeposited precursors, J. Electrochem. Soc. 145 (1998) 3435, http://dx.doi.org/10.1149/1.1838823.

[11] K. Ramasamy, M.A. Malik, N. Revaprasadu, P. O'Brien, Routes to nanostructured inorganic materials with potential for solar energy applications, Chem. Mater. 25 (2013) 3551–3569, http://dx.doi.org/10.1021/cm401366q.

[12] J. Xu, W. Wang, X. Zhang, X. Chang, Z. Shi, G.M. Haarberg, Electrodeposition of ZnSe thin film and its photocatalytic properties, J. Alloys Compd. 632 (2015) 778–782, http://dx.doi.org/10.1016/j.jallcom.2015.01.013.

[13] A. Manzoli, K.I.B. Eguiluz, G.R. Salazar-Banda, S.A.S. Machado, Electrodeposition and characterization of undoped and nitrogen-doped ZnSe films, Mater. Chem. Phys. 121 (2010) 58–62, http://dx.doi.org/10.1016/j.matchemphys.2009.12.038.

[14] A.P. Samantilleke, M.H. Boyle, J. Young, I.M. Dharmadasa, Electrodeposition of n-type and p-type ZnSe thin films for applications in large area optoelectronic devices, J. Mater. Sci. Mater. Electron. 9 (1998) 289–290, http://dx.doi.org/10.1023/A:1008876722944.

[15] C.D. Lokhande, P.S. Patil, H. Tributsch, A. Ennaoui, ZnSe thin films by chemical bath deposition method, Sol. Energy Mater. Sol. Cells 55 (1998) 379–393, http://dx.doi.org/10.1016/S0927-0248(98)00112-3.

[16] R. Kumaresan, M. Ichimura, E. Arai, Photochemical deposition of ZnSe polycrystalline thin films and their characterization, Thin Solid Films 414 (2002) 25–30, http://dx.doi.org/10.1016/S0040-6090(02)00450-9.

[17] A. Manzoli, M.C. Santos, S.A.S. Machado, A voltammetric and nanogravimetric study of ZnSe electrodeposition from an acid bath containing Zn(II) and Se(IV), Thin Solid Films 515 (2007) 6860–6866, http://dx.doi.org/10.1016/j.tsf.2007.02.030.

[18] K.R. Murali, M. Balasubramanian, Properties of pulse plated ZnSe films, Mater. Sci. Eng. A Struct. 431 (2006) 118–122, http://dx.doi.org/10.1016/j.msea.2006.05.123.

[19] M. Bouroushian, T. Kosanovic, N. Spyrellis, Aspects of ZnSe electrosynthesis from selenite and selenosulfite aqueous solutions, J. Solid State Electron. 9 (2005) 55–60, http://dx.doi.org/10.1007/s10008-004-0556-3.

[20] T. Kosanovic, M. Bouroushian, N. Spyrellis, Soft growth of the ZnSe compound from alkaline selenosulfite solutions, Mater. Chem. Phys. 90 (2005) 148–154, http://dx.doi.org/10.1016/j.matchemphys.2004.10.027.

[21] S.R. Kumar, M. Nuthalapati, J. Maity, Development of nanocrystalline ZnSe thin film through electrodeposition from a non-aqueous solution, Scripta Mater. 67 (2012) 396–399, http://dx.doi.org/10.1016/j.scriptamat.2012.05.029.

[22] G. Riveros, H. Gomez, R. Henriquez, R. Schrebler, R.E. Marotti, E.A. Dalchiele, Electrodeposition and characterization of ZnSe semiconductor thin films, Sol. Energy Mater. Sol. Cells 70 (2001) 255–268, http://dx.doi.org/10.1016/S0927-0248(01)00066-6.

[23] R. Chandramohan, T. Mahalingam, J.P. Chu, P.J. Sebastian, Preparation and characterization of electrosynthesized zinc selenide thin films, J. New Mater. Electrochem. Syst. 8 (2005) 143–148, http://dx.doi.org/10.1149/04509.0019ecst.

[24] E.B. Chubenko, A.A. Klyshko, V.A. Petrovich, V.P. Bondarenko, Electrochemical deposition of zinc selenide and cadmium selenide onto porous silicon from aqueous acidic solutions, Thin Solid Films 517 (2009) 5981–5987, http://dx.doi.org/10.1016/j.tsf.2009.03.134.

[25] M. Bouroushian, T. Kosanovic, Z. Loizos, N. Spyrellis, Electrochemical formation of zinc selenide from acidic aqueous solutions, J. Solid State Electrochem. 6 (2002) 272–278, http://dx.doi.org/10.1007/s100080100215.

[26] J.L. Yang, Z.G. Jin, Y. Shi, Z.P. Ge, Influence of mechanical agitation on ZnSe electrodeposition in H_2SeO_3 -$ZnSO_4$ aqueous solution, Adv. Appl. Ceram. 107 (2008) 350–353, http://dx.doi.org/10.1179/174367508X297795.

[27] C. Natarajan, M. Sharon, C. Levy-Clement, M. Neumann-Spallart, Electrodeposition of zinc selenide, Thin Solid Films 237 (1994) 118–123, http://dx.doi.org/10.1016/0040-6090(94)90247-X.

[28] T. Mahalingam, A. Kathalingam, S. Velumani, S. Lee, M.H. Sun, K.Y. Deak, Electrochemical synthesis and characterization of zinc selenide thin films, J. Mater. Sci. 41 (2006) 3553–3559, http://dx.doi.org/10.1007/s10853-005-5622-4.

[29] Geometrical Product Specifications (GPS), Surface texture: profile method—metrological characteristics of phase correct filters, Standard ISO 11562, International Organization for Standardization, 1996.

[30] I.T. McCrum, M.J. Janik, pH and alkali cation effects on the Pt cyclic voltammogram explained using density functional theory, J. Phys. Chem. C 120 (1) (2016) 457–471.

[31] M. Grdeń, A. Piaścik, Z. Koczorowski, A. Czerwiński, J. Electroanal. Chem. 532 (2002) 35–42.

[32] J.M. Feliu, R. Gómez, M.J. Llorca, A. Aldaz, Electrochemical behavior of irreversibly adsorbed selenium dosed from solution on Pt(h,k,l) single crystal electrodes in sulphuric and perchloric acid media, Surf. Sci. 289 (1993) 152–162.

[33] S. Soundeswaran, O.S. Kumar, R. Dhanasekaran, P. Ramasamy, R. Kumaresen, M. Ichimura, Growth of ZnSe thin films by electrocrystallization technique, Mater. Chem. Phys. 82 (2003) 268–272, http://dx.doi.org/10.1016/S0254-0584(03)00226-8.

[34] K.R. Murali, V.S. Vidya, M. Jayachandran, Properties of ZnSe films pulse electrodeposited in the presence of phosphotungstic acid, Ionics 14 (2008) 569–575, http://dx.doi.org/10.1007/s11581-008-0221-4.

[35] A. Kassim, H.S. Min, T.W. Tee, A. Shariff, N. Saravanan, Chemical bath deposition of ZnSe thin films: SEM and XRD characterization, European J Appl. Sci. 3 (2011) 113–116.

[36] A.L. Fahrenbruch, II–VI compounds in solar energy conversion, J. Cryst. Growth 39 (1977) 73–91, http://dx.doi.org/10.1016/0022-0248(77)90156-7.

[37] N.A. Okereke, A.J. Ekpunobi, ZnSe buffer layer deposition for solar cell application, J. Non-Oxide Glasses 3 (2011) 31–36.

[38] S.N. Guin, D. Sanyal, K. Biswas, The effect of order–disorder phase transitions and band gap evolution on the thermoelectric properties of AgCuS nanocrystals, Chem. Sci. 7 (2016) 534–543, http://dx.doi.org/10.1039/C5SC02966J.

[39] V. Dhanasekaran, T. Mahalingam, J.K. Rhee, J.P. Chu, Structural and optical properties of electrosynthesized ZnSe thin films, Optik 124 (2013) 255–260, http://dx.doi.org/10.1016/j.ijleo.2011.11.063.

[40] P.C. Pingale, S.T. Mane, R.V. Suryawanshi, L.P. Deshmukh, Structural, morphological and optical studies of ZnSe thin films: growth using chemical bath, Adv. Appl. Sci. Res. 4 (2013) 177–181.

[41] K. Singh, J.P. Rai, Photoelectric conversion studies on zinc selenide, J. Mater. Sci. 22 (1987) 132–136, http://dx.doi.org/10.1007/BF01160561.